ORIGINAL PAPER

RJME Romanian Journal of Morphology & Embryology http://www.rjme.ro/

Comparative histochemical and immunohistochemical assessment of cardiac alterations in high-fat diet-fed rats treated with semaglutide *vs.* tirzepatide

HARITH ALI HASAN, LUMA IBRAHIM AL-ALLAF

Department of Anatomy, College of Medicine, University of Mosul, Iraq

Abstract

Background: Cardiac remodeling in obesity is a complex phenomenon involving myocardial fibrosis, inflammatory infiltration, lipotoxicity and vascular changes. Incretin-based anti-obesity medications, such as tirzepatide and semaglutide, are drugs that have been proposed to have potential cardiometabolic effects, but there is a scarcity of preclinical head-to-head histological comparisons. The objectives are to characterize the histochemical and immunohistochemical cardiac tissue alterations in high-fat diet (HFD)-induced obese rats after subcutaneous administration of semaglutide or tirzepatide daily for 28 days and quantify the tissue and serum monocyte chemoattractant protein-1 (MCP-1) as an inflammatory marker. *Materials and Methods*: Forty adult male Wistar rats were assigned to four groups (n=10): control, obese, obese+semaglutide, and obese+tirzepatide. Cardiac tissue was then evaluated by Hematoxylin and Eosin (H&E), Masson's trichrome (MT) and immunohistochemistry [cluster of differentiation (CD)31, CD36, CD86] and collagen area fraction and immunopositive area were quantified using digital image analysis (ImageJ). Levels of MCP-1 were determined in serum and tissues by enzyme-linked immunosorbent assay (ELISA). *Results*: Mean weekly weight gain was seen to increase in the obese rats (376.9±37.67 g at week 4 of treatment), adipocyte-like clear spaces were observed in the cardiac valve layers, collagen area fraction increased in the cardiac valve, myocardial ventricles, and coronary artery wall, MCP-1 mean level was elevated in serum and tissues (control *vs.* obese), and CD36 and CD86 immunopositivity increased and CD31 immunopositivity decreased in the cardiac valve, myocardial ventricles and coronary artery wall compared to control rats. The body weight, collagen area fraction, CD36, and CD86 immunopositivity were lower, and MCP-1 was lower, in both treated groups *vs.* the obese group, with numerically greater reductions in the tirzepatide group (serum MCP-1: 463.8±4.71 pg/mL; tissue MCP-1: 330.80±18.17 pg/mg). However, intermediate changes but with residual fibrosis were seen in the presence of semaglutide. *Conclusions*: Tirzepatide was associated with more favorable changes in cardiac histomorphology and in the markers assessed compared with semaglutide in this four-week model, suggesting a potential cardioprotective association that warrants further mechanistic investigation.

Keywords: cardiac tissue, semaglutide, tirzepatide, MCP-1, Masson's trichrome, immunohistochemistry.

Introduction

Obesity has become one of the most pressing global health crises of the 21st century, affecting more than 650 million adults worldwide according to the *World Health Organization* [1]. Beyond its metabolic consequences, obesity imposes a profound burden on the cardiovascular (CV) system, contributing to heart failure, coronary artery disease, arrhythmias, and sudden cardiac death [2, 3]. The pathological remodeling of cardiac tissue in obese individuals termed obesity-associated cardiac remodeling, encompasses a spectrum of structural and functional abnormalities including myocardial hypertrophy, interstitial fibrosis, valvular remodeling, and microvascular dysfunction [4, 5].

At the cellular and molecular level, obesity-related cardiac injury is thought to be mediated by several interacting mechanisms. Ectopic lipid accumulation within cardiomyocytes, facilitated by the fatty acid (FA) translocase cluster of differentiation (CD)36, has been linked to intramyocardial ceramide and diacylglycerol synthesis, mitochondrial dysfunction, oxidative stress, and cardiomyocyte apoptosis [6, 7]. In parallel, a state of low-grade cardiac inflammation can be sustained by the recruitment of circulating monocytes *via* monocyte chemoattractant protein-1 [MCP-1/C–C motif chemokine ligand 2 (CCL2)] and their differentiation into proinflammatory macrophages; CD86 is one of several co-stimulatory molecules used to identify such macrophages, although it is not macrophage-specific [8, 9]. These macrophages can secrete cytokines including interleukin (IL)-1β, tumor necrosis factor-alpha (TNF)-α and IL-6 that sustain a fibrotic environment and impair endothelial function [10, 11]. Vascular changes are also relevant: obesity has been associated with impaired endothelial integrity and coronary angiogenesis, which may reduce myocardial perfusion reserve and capillary density [12]. CD31 [platelet endothelial cell adhesion molecule-1 (PECAM-1)], expressed on endothelial cells, is an endothelial lineage and adhesion marker used as one indicator of vascular density and endothelial integrity [13].

In recent years, incretin-based therapies have emerged as important agents in the management of obesity and cardiometabolic disease. Semaglutide, a glucagon-like peptide-1 (GLP-1) receptor agonist, was initially developed for type 2 diabetes but has since demonstrated substantial weight-loss efficacy; a comparable CV benefit was previously reported in a diabetic population in the SUSTAIN-6 trial [14]. In

This is an open-access article distributed under the terms of a Creative Commons Attribution-NonCommercial-ShareAlike 4.0 International Public License, which permits unrestricted use, adaptation, distribution and reproduction in any medium, non-commercially, provided the new creations are licensed under identical terms as the original work and the original work is properly cited.

the SELECT trial, semaglutide reduced major adverse CV events by 20% in patients with overweight or obesity and established CV disease but without diabetes [hazard ratio (HR) 0.80, 95% confidence interval (CI) 0.72–0.90] [15]. Over the last few years, incretin-based therapies have become significant drugs for the treatment of obesity and cardiometabolic diseases. Tirzepatide, a dual glucose-dependent insulinotropic polypeptide (GIP)/GLP-1 receptor agonist (dual GIP/GLP-1 receptor agonist), has been shown to cause greater weight reduction than placebo in the SURMOUNT-1 trial [16] and greater weight and waist-circumference reduction than semaglutide in the head-to-head SURMOUNT-5 trial [17]; dedicated CV-outcome trials for tirzepatide are still pending, and a direct CV-outcome comparison with semaglutide is not yet available. The dual-receptor effect of tirzepatide beyond GLP-1 receptor agonism in providing cardiometabolic benefits is still uncertain [18].

Although this increased clinical evidence exists, there is to our knowledge no direct comparison of these two drugs on cardiac tissue, that has been made in a common experimental animal model. Comparisons of this type could be used to formulate hypotheses concerning the tissue-level differences that might underlie clinical differences between the two agents [19, 20].

Aim

Based on this, this study aimed to characterize cardiac tissue characteristics in a high-fat diet (HFD) induced rat obesity model and compare the changes observed following subcutaneous (s.c.) injection with semaglutide or tirzepatide in cardiac valve, the ventricular myocardium and coronary artery.

Materials and Methods

Ethical approval

All experimental procedures were conducted in full compliance with the ethical principles for the use of laboratory animals and were approved by the Institutional Animal Care and Use Committee (IACUC) of the College of Medicine, University of Mosul, Iraq (Approval No. UOM-IACUC-2023/147). Animals were maintained under standard conditions and received humane care in accordance with the guidelines of the *National Institutes of Health* (NIH) Guide for the Care and Use of Laboratory Animals [21].

Experimental animal

Forty adult male Wistar rats (body weight 230–265 g, aged 10–12 weeks) were obtained from the Animal House of the College of Medicine, University of Mosul. Animals were acclimatized for one week under controlled environmental conditions (ambient temperature 22±2°C, relative humidity 55±5%, 12-hour light/dark cycle) with free access to water. All animals were individually weighed on an electronic balance at the same time each day throughout the study period. Rats were randomly allocated into four groups of 10 animals each, as follows:

- Group I – control (n=10): standard rodent chow (3.8 kcal/g) for 12 weeks;
- Group II – obese/HFD (n=10): HFD (60% kcal from fat) for 12 weeks;
- Group III – obese+semaglutide (n=10): HFD for 12 weeks + daily s.c. semaglutide (0.12 mg/kg/day, Ozempic®, Novo Nordisk) for 28 days [22];
- Group IV – obese+tirzepatide (n=10): HFD for 12 weeks + daily s.c. tirzepatide (0.05 mg/kg/day, Mounjaro®, Eli Lilly) for 28 days [23].

Body weights were collected on day 1 of drug/vehicle injection (baseline), and at the end of each week, for four weeks. For this manuscript, the term “baseline” is used to indicate this treatment initiation time point, and not the time point the overall 12-week protocol is initiated.

Sample size

The number of animals (n=10) per group was determined by reference to similar published rodent cardiometabolic studies and not using a power analysis for the primary endpoints of this study. No animals were excluded from the final analysis, and no animals had adverse events or attrition throughout the duration of treatment.

Dose selection and administration schedule

Semaglutide and tirzepatide are both approved for once-weekly dosing in humans, but both agents were administered once daily in this study. This was based on the substantially shorter half-life of both peptides in rats than in humans: in humans, the half-life of semaglutide is ≈155–183 hours (~1 week) and that of tirzepatide is ≈5 days, allowing once-weekly dosing, largely because both molecules are engineered to bind albumin *via* a FA chain, which slows renal clearance [24, 25]. In rats, this albumin-binding prolongation is considerably less effective, and reported half-lives are much shorter approximately 7.22–9.26 hours for semaglutide reflecting the faster metabolic rate and renal/hepatic clearance of rodents relative to body weight, and species differences in albumin-binding and s.c. absorption kinetics [24, 25]. Because the rat half-life is roughly 20-fold shorter than the human half-life, a single weekly dose in rats would produce a very sharp decline in plasma concentration between doses, and once-daily dosing was therefore used to maintain more continuous drug exposure across the four-week treatment period [24, 25]. This pharmacokinetic rationale explains why daily dosing was chosen, but it does not by itself establish that the two doses used here are pharmacodynamically equivalent between the two drugs; doses were selected from the cited preclinical literature [22, 23] rather than derived by direct allometric/exposure scaling from the approved human doses, and the two doses have not been confirmed to produce equivalent systemic exposure in rats. This is outlined further below as a study limitation. The dose of Ozempic® (semaglutide) was diluted so that each 1 mL of solution contained 1.34 mg of semaglutide in 29 mL of normal saline and each animal (~300 g body weight) received 0.1 mL (0.12 mg/kg). Each 0.6 mL of Mounjaro® stock solution was diluted in 60 mL of normal saline, resulting in 15 mg of Mounjaro® per 60 mL. Each animal (around 300 g body weight) was given 0.1 mL (0.05 mg/kg) of Mounjaro® stock solution. The diluted preparations were kept at 4°C and each animal was given an s.c. injection at the same time of day (10:00 AM) into the skin of the back over the neck-fold. Control and obese groups were not injected daily with sham/vehicle injections, which is recognized as a study limitation in the “Discussions”

section, as handling and injection stress was not equalized between the groups.

Induction of obesity

Obesity was induced by administering an HFD consisting of 60% kcal from fat, 20% from protein, and 20% from carbohydrates (Research Diets, D12492) for eight consecutive weeks prior to drug administration. Obesity was confirmed at the initiation of the injection phase when HFD-fed rats achieved body weight ≥20% above the mean of control animals, consistent with established rodent obesity criteria [26, 27]. Overall, the protocol included: a one-week acclimatization period; eight-week obesity induction period (control on standard chow, all other groups on HFD); confirmation of obesity at week 8; randomization of obese animals into the obese, semaglutide, and tirzepatide treatment groups; four-week treatment period (weeks 9–12) receiving HFD (or standard chow for control) concurrently with daily injections; and terminal collection of blood and tissues at the end of week 12.

Tissue preparation and histological staining

Animals were anaesthetized at the end of treatment with a combination of ketamine (80 mg/kg) and xylazine (10 mg/kg) and absence of the pedal withdrawal reflex was used to confirm depth of anesthesia. The second method of euthanasia was cervical dislocation in accordance with guidelines from the *American Veterinary Medical Association* (AVMA) [28]. Median sternotomy was performed, and a rapid removal of the heart was performed, which was weighed (Table 1); relative heart weight (%) was calculated as (heart weight [g]/body weight [g]) × 100. Cardiac tissues were fixed in 10% neutral buffered formalin for 48 hours, then routinely processed through ascending grades of ethanol, cleared in xylene, and embedded in paraffin wax. Sequential coronal sections of 5 μm were cut on a rotary microtome.

Tissue sections were stained with Hematoxylin and Eosin (H&E) for general histological morphology. Masson's trichrome (MT) staining was performed to visualize collagen fibers (blue/green) and muscle fibers (red/pink), enabling semi-quantitative assessment of fibrosis in cardiac valves, ventricular myocardium, and coronary artery walls [29].

Valve sections were sampled from a standardized coronal level of the mitral valve, with orientation and the anatomical landmarks used to identify the *fibrosa*, *spongiosa*, and *ventricularis* layers kept consistent across animals within each staining batch.

Immunohistochemistry

Paraffin sections were deparaffinized in xylene and rehydrated through graded alcohols. Antigen retrieval was performed in 0.01 M sodium citrate buffer (pH 6.0) at 95°C for 20 minutes in a water bath. Endogenous peroxidase activity was blocked with 3% hydrogen peroxide (H_2O_2) in methanol for 10 minutes. Non-specific binding was blocked with normal goat serum (5%, 30 minutes). Primary antibody incubations were performed overnight at 4°C using the following antibodies: anti-CD31/PECAM-1 (Abcam, ab28364, rabbit polyclonal, 1:200), endothelial cell marker; anti-CD36 (Abcam, ab133625, rabbit monoclonal, 1:150), FA translocase/scavenger receptor; anti-CD86 (Abcam, ab213044, rabbit monoclonal, 1:200), co-stimulatory marker used here as a component of macrophage identification.

Secondary antibody incubation used horseradish peroxidase (HRP)-conjugated goat anti-rabbit immunoglobulin G (IgG) (1:500, 45 minutes at room temperature). Visualization was achieved with 3,3'-diaminobenzidine (DAB) chromogen (brown precipitate). Sections were counterstained with Mayer's Hematoxylin, dehydrated, and coverslipped with DPX mountant. Negative controls [primary antibody omitted and replaced with phosphate-buffered saline (PBS)] were included in all runs. Immunoreactivity was scored semi-quantitatively by two independent, blinded observers [30]. The primary quantitative measurements (with associated group comparisons) reported in the text and listed in Tables 2 and 3 are the collagen area fraction and percentage DAB-positive area/integrated optical density (IOD) that were obtained using the ImageJ software to perform a quantitative analysis.

Digital image analysis (ImageJ)

To complement the semi-quantitative visual scoring, all MT and immunohistochemical (IHC) (CD31, CD36, CD86) photomicrographs were additionally analyzed digitally using ImageJ software (version 1.54, *NIH*, Bethesda, MD, USA), a widely used open-source platform for quantitative histological image analysis [31].

For MT sections, five non-overlapping fields per animal (valve, ventricular myocardium, and coronary artery compartments) were captured at standardized magnification and illumination settings. Images were converted to red, green and blue (RGB) format and processed in ImageJ to separate the collagen (blue/green) component from the muscle/cytoplasmic (red) component; the collagen area fraction (percentage of blue/green-stained area relative to total tissue area in each two-dimensional field; this measure is reported here as an area fraction rather than a true stereological volume fraction) was calculated for each field [32]. The mean value across the five fields was used as the single value per animal for intergroup statistical comparison, *i.e.*, the animal not the individual field was the statistical unit.

For CD31, CD36, and CD86 immunostained sections, DAB-positive (brown) immunoreactivity was similarly quantified by ImageJ color deconvolution to separate the DAB chromogen signal from the Hematoxylin counterstain. The percentage of DAB-positive area and the IOD were computed for five random high-power fields per animal using threshold-based area-fraction analysis, an approach consistent with the IHC Profiler method for semi-automated scoring of immunohistochemistry images [33]. Again, the five-field mean per animal was used as the unit of analysis. An observer blind to group allocation acquired and analyzed images. To capture the differences between the groups, a single, fixed color deconvolution vector and threshold range were used across all images of each stain, with the threshold fine-tuned by the observer, image by image, within this fixed range to capture the trichrome/DAB-positive signal as seen on each slide, thus providing a degree of control over the differences in staining-intensity which was generated by the manual staining procedure used. This fine-tuning operation still involved some degree of observer judgment, so it cannot be said to be completely observer independent [34].

MCP-1 quantification

Blood was aspirated from the ophthalmic venous plexus using a micropipette [35], before euthanasia, allowed to clot,

and centrifuged at 3000 rpm for 10 minutes; serum was stored at -20°C. Cardiac tissue was homogenized in ice-cold PBS (100 mg tissue/mL) using a tissue homogenizer, centrifuged at 10 000×g for 15 minutes, and the supernatant collected. The level of rat MCP-1 was determined by a commercial sandwich enzyme-linked immunosorbent assay (ELISA) kit, in which 50 µL of standard or 10 µL of serum/tissue extract plus 40 µL of sample diluent were added per well, followed by 100 µL of HRP–conjugate reagent per well; the plates were covered and incubated for 60 minutes at 37°C, then washed five times using a manifold dispenser with thorough removal of the wash buffer between each wash. Then 50 µL of chromogen solution A and B were put into each well and plates were incubated at 37°C in the dark for 15 minutes, after which 50 µL of stop solution was added to each well (color change blue to yellow). The optical density was measured at 450 nm within 15 minutes using a microplate reader. Tissue MCP-1 was normalized to total protein content determined by Bradford assay (Bio-Rad, USA). Results are expressed as pg/mL (serum) and pg/mg protein (tissue) [36].

Statistical analysis

All data are presented as mean ± standard deviation (SD). Intergroup differences at each individual time point, and in IHC scores and ImageJ-derived quantitative parameters (collagen area fraction, % DAB-positive area), were assessed using one-way analysis of variance (ANOVA) followed by Tukey's honestly significant difference (HSD) *post-hoc* test for normally distributed data, or the Kruskal–Wallis *H*-test followed by Dunn's *post-hoc* correction for non-normally distributed data. Statistical significance was set at $p<0.05$. All analyses were conducted using Statistical Package for the Social Sciences (SPSS) version 26.0 (IBM Corp., Armonk, NY, USA) [37]. Repeated body weight measurements over time were analyzed by one-way ANOVA, with Tukey's HSD *post-hoc* correction for pairwise comparisons among groups at each individual week, separately at each week rather than by a repeated-measures or mixed-effects model that would account for within-animal correlation across time points.

Results

At treatment baseline (start of week 9), all three HFD groups had significantly higher body weights than controls ($p<0.05$), confirming successful obesity induction (Figure 1). The obese group demonstrated continuous and progressive weight gain throughout the study period, reaching 376.9 ±37.67 g by treatment week 4. In contrast, both treatment groups exhibited significant and progressive weight reduction beginning from week 1. By week 4, tirzepatide-treated rats weighed 258.7±32.45 g and semaglutide-treated rats weighed 259.2±22.8 g, values not significantly different from the control group (265.4±32.46 g; $p>0.05$). No statistically significant difference was found between tirzepatide and semaglutide groups at any time point ($p>0.05$). To support the difference in the slopes of weight gain and weight loss among groups, one-way ANOVA with Tukey's HSD *post-hoc* correction was performed at each individual weekly time point. This week-by-week testing supports the divergence of the treatment slopes from the obese trajectory from an early time point, and not just at the end of treatment.

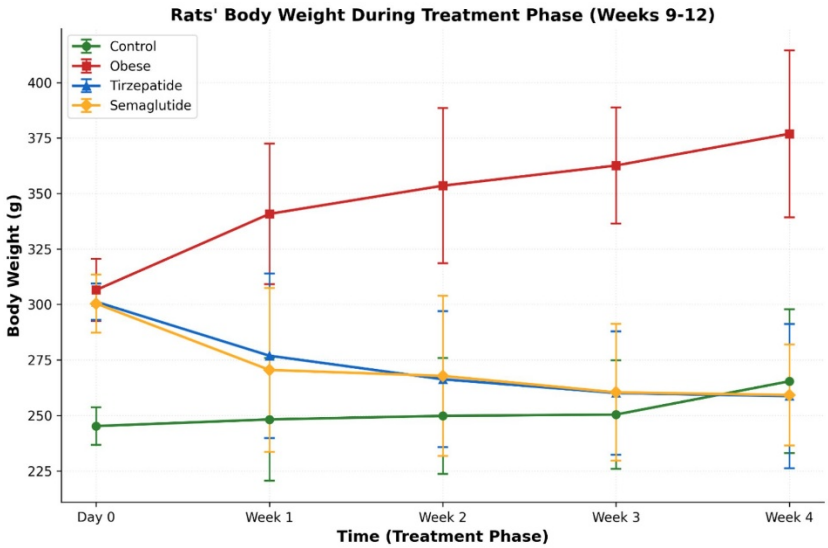

Figure 1 – ***Body weight (g) across four weeks of daily subcutaneous treatment. Group order: control, obese, tirzepatide, semaglutide (n=10/group). Values are mean ± SD. *p<0.05 vs. control; †p<0.05 vs. obese (one-way ANOVA with Tukey's HSD post-hoc, each week). ANOVA: Analysis of variance; HSD: Honestly significant difference; SD: Standard deviation.***

Heart weight

Obesity caused by the HFD resulted in a significant 36.4% increase in absolute heart weight (1.108±0.053 g *vs.* 0.8125±0.09 g in controls; $p<0.001$). There was a significant decrease in weight compared to obese group for both tirzepatide (0.847±0.094 g) and semaglutide (0.800±0.095 g), which were comparable with the control group ($p>0.05$; Figure 2, A and B; Table 1). Relative heart weight was also paradoxically lower in the obese group (0.279±0.0155%) than in controls (0.3058±0.0195%), due to the disproportionately increased amount of total body weight compared to heart weight. The relative heart weight of both treatment groups did not differ from controls ($p>0.05$) (Table 1).

Table 1 – ***Heart weight and relative heart weight***

Parameter	Control	Obese	Tirzepatide	Semaglutide
Absolute heart weight [g]	0.8125± 0.09	1.108± 0.053***	0.847± 0.094†	0.800± 0.095†
Relative heart weight [g]	0.3058± 0.0195	0.279± 0.0155	0.3066± 0.0251	0.2926± 0.0172

Group order: control, obese, tirzepatide, semaglutide (*n*=10/group). Values are mean ± SD. ***p<0.001 *vs.* control; †p<0.05 *vs.* obese. *n*: No. of animals; SD: Standard deviation.

Group order, control, obese, tirzepatide, semaglutide, matching are illustrated in Figure 2 (A and B) and Figure 3 (A and B).

MCP-1 level

Serum MCP-1 was significantly higher in the obese group (525.78±40.13 pg/mL) than in controls (409.33±48.81 pg/mL; p<0.001). The serum concentration of MCP-1 was significantly lower in both tirzepatide (463.8±4.71 pg/mL) and semaglutide (487.0±8.29 pg/mL) groups compared with the obese group (p<0.05), with a significantly greater decrease in the tirzepatide group (p<0.05 *vs.* semaglutide). Cardiac tissue MCP-1 followed a parallel pattern: highest in the obese group (366.86±15.64 pg/mg), followed by the semaglutide (352.35±8.83 pg/mg), tirzepatide (330.80±18.17 pg/mg), and control (286.17±22.14 pg/mg) groups (Figure 3, A and B).

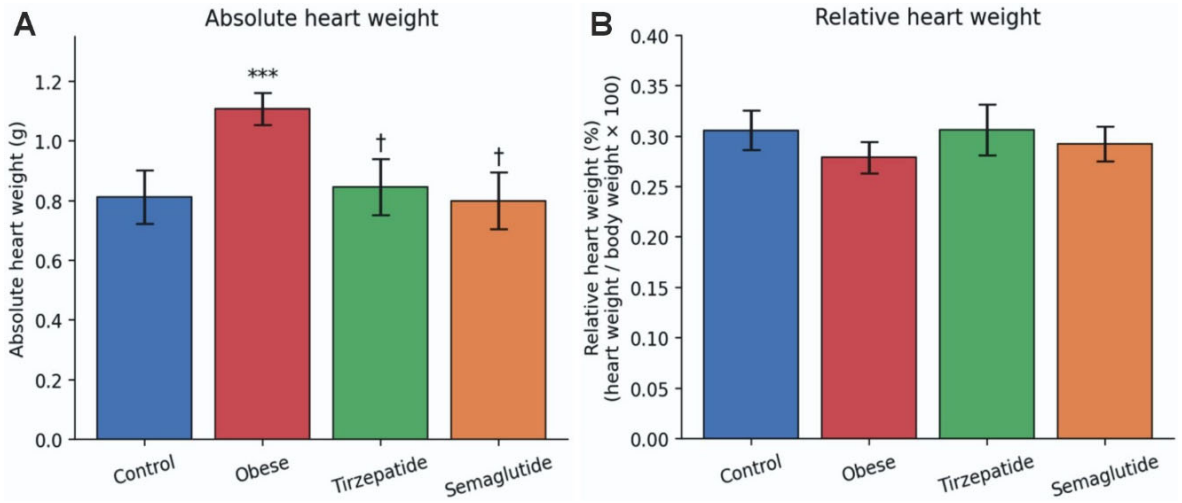

Figure 2 – ***Absolute (A) and relative (B) heart weight across experimental groups, corresponding to Table 1. Group order: control, obese, tirzepatide, semaglutide (n=10/group). Values are mean ± SD. ***p<0.001 vs. control; †p<0.05 vs. obese. SD: Standard deviation.***

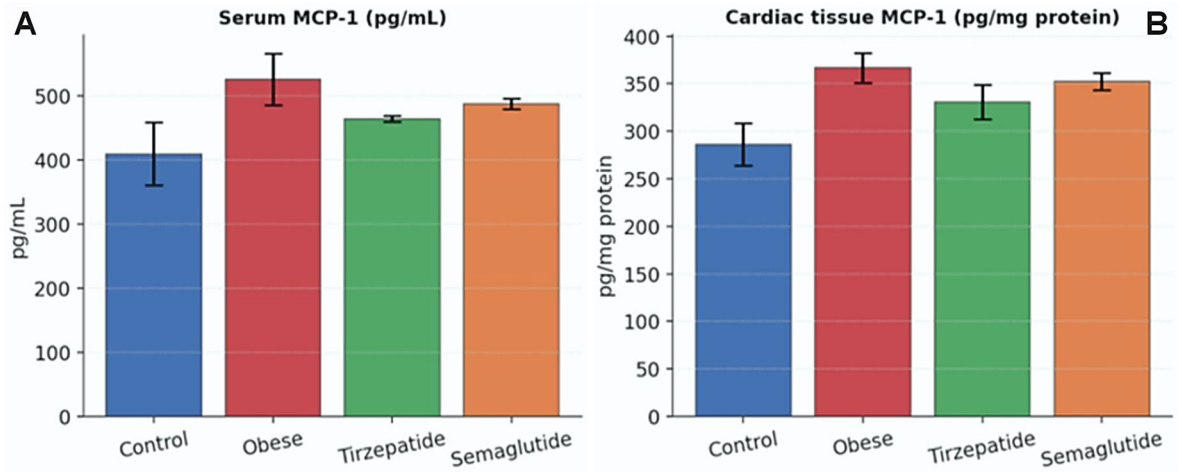

Figure 3 – ***Serum (A) and cardiac tissue (B) MCP-1 levels across experimental groups. Group order: control, obese, tirzepatide, semaglutide (n=10/group), matching Figures 1–3 and Table 1. Values are mean ± SD. ***p<0.001 vs. control; †p<0.05 vs. obese; ‡p<0.05 tirzepatide vs. semaglutide (one-way ANOVA with Tukey's HSD post-hoc). ANOVA: Analysis of variance; HSD: Honestly significant difference; MCP-1: Monocyte chemoattractant protein-1; SD: Standard deviation.***

Histological finding (H&E staining)

Heart valve architecture

Control group

H&E-stained sections of the cardiac valve revealed normal three-layered architecture. The *fibrosa* layer at the aortic side displayed dense, organized fibrous connective tissue. The *spongiosa* layer occupied the central zone with loose connective tissue and scattered glycosaminoglycans. The *ventricularis* layer at the ventricular surface appeared thin and regular. No inflammatory infiltration or adipocyte-like clear spaces were observed (Figure 4A).

Obese group

Marked structural disruption of the valve layers was evident. There was pronounced thickening of both the

spongiosa and *ventricularis* layers. Cell poor spaces with large, clear vacuoles, morphologically consistent with mature adipocytes were identified within the *spongiosa* layer, disrupting its normal extracellular matrix (ECM). Dense inflammatory cell infiltration was observed, particularly at the *spongiosa–ventricularis* interface, with clusters of mononuclear leukocytes (Figure 4B).

Semaglutide-treated group

Partially there was an improvement in valve architecture. *Fibrosa* layer showed mild thickening on the aortic side with near normal thickness of the *spongiosa* and *ventricularis* layers. Occasionally, residual inflammatory cells were seen but were decreased in number from the obese group. There were no adipocyte-like clear spaces found (Figure 4C).

Tirzepatide-treated group

Thickness and cellularity of the valve architecture in the tirzepatide-treated group appeared to be comparable to the control group, with almost complete restoration of the three-layered structure (*fibrosa*, *spongiosa*, *ventricularis*). There was no inflammatory infiltration, or adipocyte-like clear spaces, noted (Figure 4D).

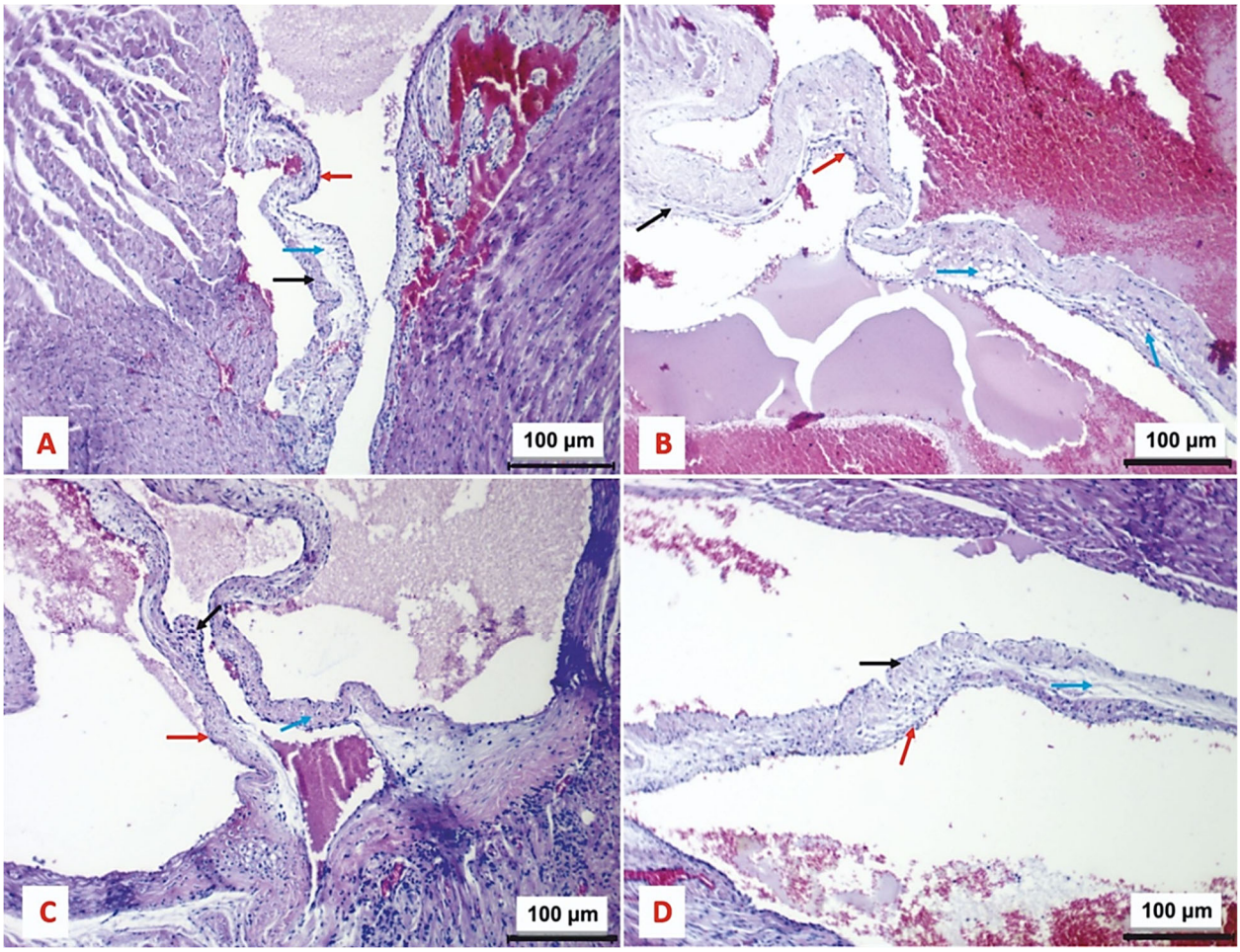

Figure 4 – ***Histological section of cardiac valve (H&E staining): (A) Control group showing normal thickness of the three layers: fibrosa layer at the aortic side (black arrow), spongiosa layer in the middle (blue arrow), and ventricularis layer at the ventricular side (red arrow); no inflammatory cells or adipocyte-like clear spaces; (B) Obese group showing an abnormal increase in thickness of the spongiosa and ventricularis layers (black arrow), clear spaces morphologically consistent with mature adipocytes within the spongiosa layer (blue arrows), and infiltration of inflammatory cells (red arrow); (C) Semaglutide group showing residual thickening of the fibrosa layer at the aortic side (black arrow), near-normal spongiosa in the middle (blue arrow), and near-normal ventricularis layer at the ventricular side (red arrow); (D) Tirzepatide-treated group showing near-complete restoration of the three-layered architecture: fibrosa (black arrow), spongiosa (blue arrow), and ventricularis (red arrow), comparable to the control group; no inflammatory cells or adipocyte-like clear spaces. Scale bar: (A–D) 100 µm. H&E: Hematoxylin and Eosin.***

Histochemical finding (MT staining)

Cardiac valve architecture

Control group

MT staining demonstrated well-organized collagen fibers of normal thickness within all three valve layers without dense pathological fibrosis. Collagen appeared evenly distributed within the *fibrosa*, consistent with normal valve biomechanics (Figure 5A).

Obese group

Prominent disorganization and increased density of

collagen fibers were evident across all valve layers, with dense blue-staining fibrotic tissue occupying areas normally devoid of collagen. The *spongiosa* and *ventricularis* layers showed notable collagen deposition replacing normal ECM (Figure 5B).

Semaglutide-treated group

Some disordering of collagen fibers persisted in the valve layers with focal areas of blue-staining fibrotic tissue, particularly in the *fibrosa* at the aortic side. The extent of fibrosis was reduced compared with the obese group but did not fully normalize (Figure 5C).

Tirzepatide-treated group

A largely normal, organized collagen thickness was observed across all three valve layers without dense blue-staining fibrotic tissue, closely resembling the control group (Figure 5D).

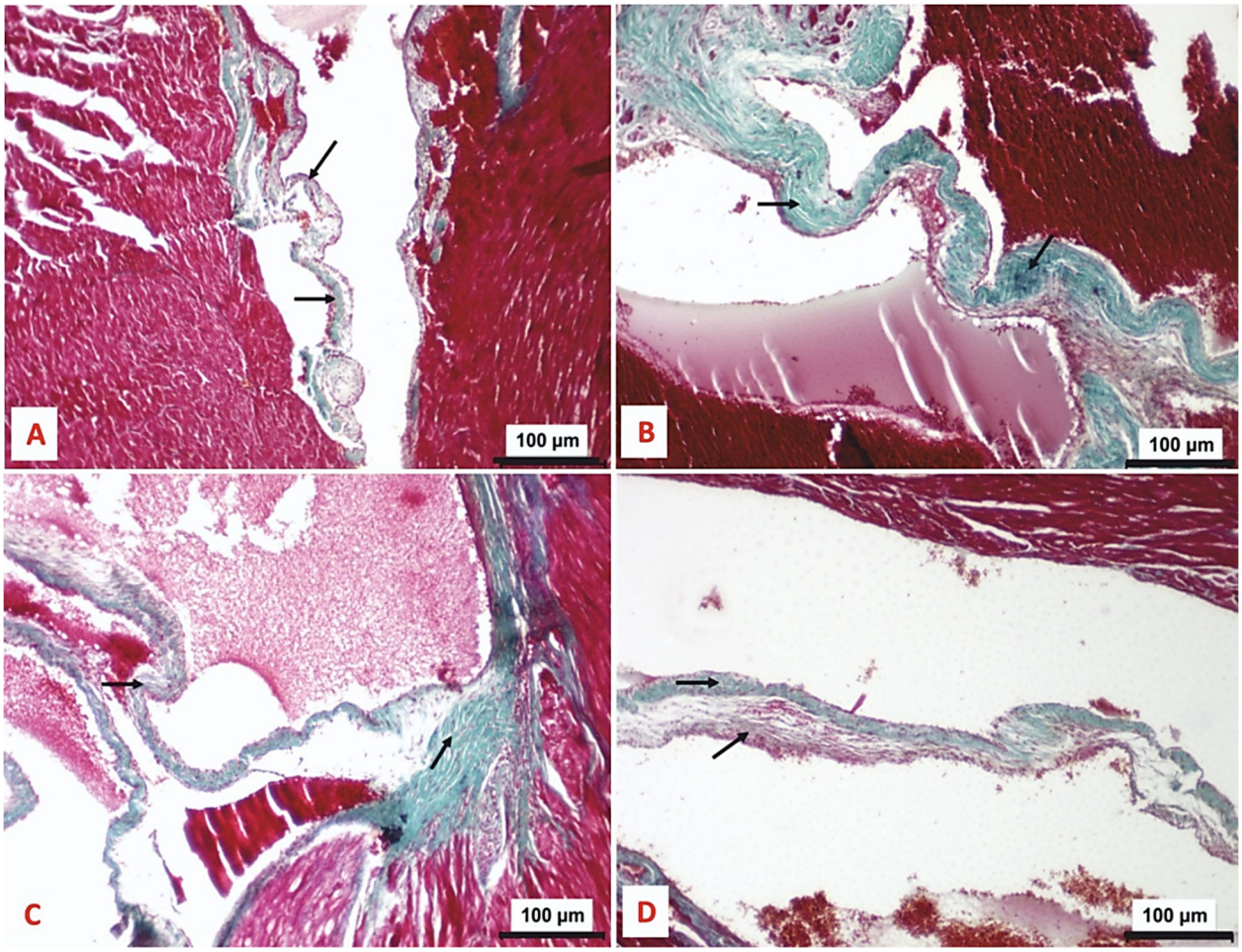

Figure 5 – ***MT staining of cardiac valve: (A) Control group showing normal, organized collagen thickness across all three valve layers without dense blue-staining fibrotic tissue (black arrows); (B) Obese group showing disorganized, dense blue-staining fibrotic tissue across the three valve layers (black arrows), consistent with fibrotic remodeling; (C) Semaglutide group showing some residual disordered collagen fiber arrangement in the valve layers with focal dark blue-staining fibrotic tissue in some areas (black arrows); (D) Tirzepatide group showing a largely normal, organized collagen thickness across all three valve layers without dense blue-staining fibrotic tissue (black arrows). Scale bar: (A–D) 100 µm. MT: Masson's trichrome.***

Cardiac ventricle

Control group

Myocardial fibers in the ventricle were arranged in a regular, parallel pattern. MT staining confirmed the absence of interstitial or perivascular collagen deposition in the myocardium (Figure 6A).

Obese group

Abnormal spreading of collagen fibers was evident around congested blood vessels (perivascular fibrosis). Cardiomyocytes showed irregular arrangement with widened interstitial spaces occupied by collagen, consistent with interstitial fibrosis (Figure 6B).

Semaglutide-treated group

Mild persistence of perivascular collagen was observed, though reduced compared with the obese group. Myocardial fiber arrangement was partially restored (Figure 6C).

Tirzepatide-treated group

A near-normal myocardial fiber arrangement was observed with little collagen deposition in the interstitium or around blood vessels, comparable to the control group (Figure 6D).

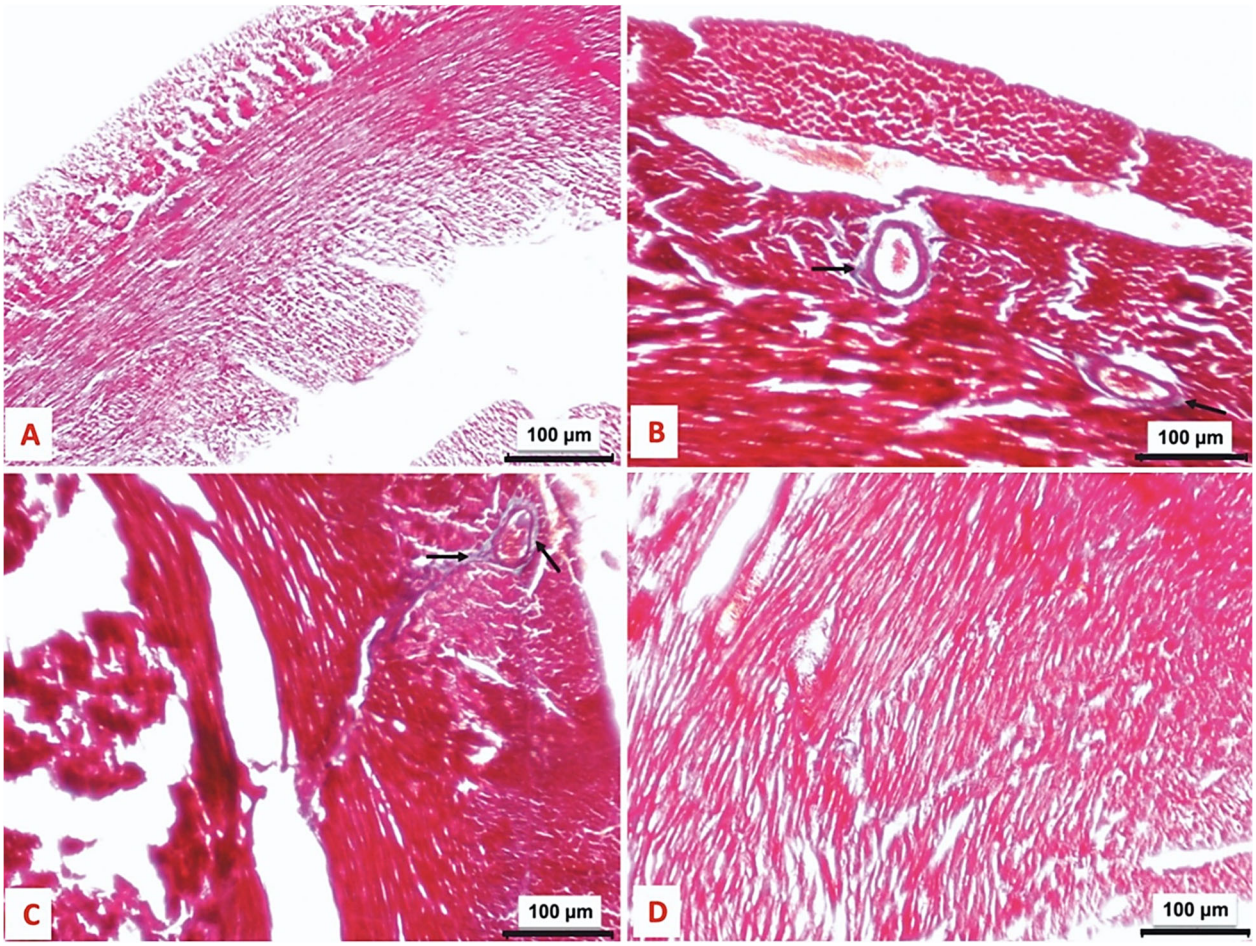

Figure 6 – ***MT staining of heart ventricle: (A) Control group showing normal myocardial fibers arranged in a regular pattern without collagen fibers in the interstitium or perivascular space; (B) Obese group showing abnormal spreading of collagen fibers around congested blood vessels (perivascular fibrosis, black arrow) and widened interstitial spaces with collagen deposition; (C) Semaglutide group showing mild residual perivascular collagen fibers around blood vessels (black arrow) with partial restoration of myocardial fiber arrangement; (D) Tirzepatide group showing a near-normal myocardial fiber arrangement with little collagen deposition, comparable to the control group. Scale bar: (A–D) 100 µm. MT: Masson's trichrome.***

Coronary artery

Control group

Collagen fibers were normally confined to the *tunica adventitia* of coronary arteries. The *tunica intima* and *media* were devoid of pathological collagen accumulation (Figure 7A).

Obese group

Markedly abnormal, thickened collagen fibers were observed in the *tunica intima* of coronary arteries, a pattern that may be consistent with early atherosclerotic-type intimal remodeling, although this was not confirmed with dedicated atherosclerosis markers or lipid staining. The adventitial collagen was also disproportionately increased (Figure 7B).

Semaglutide-treated group

Coronary artery collagen was largely restored to adventitial localization with minimal residual intimal involvement (Figure 7C).

Tirzepatide-treated group

Coronary artery collagen distribution was largely confined to the *tunica adventitia*, similar to controls (Figure 7D).

ImageJ quantification of collagen area fraction

The collagen area fraction was computed for each cardiac compartment using ImageJ and presented in Table 2. The collagen area fraction was lowest in the control group, significantly higher in the obese group, and decreased in both treatment groups, more so in the tirzepatide group than the semaglutide group, compared with the control group. One-way ANOVA (or Kruskal–Wallis where the normality assumption was not met) with *post-hoc* correction confirmed significant intergroup differences in each compartment ($p<0.05$, full pairwise results in Table 2).

Table 2 – ***Collagen area fraction by MT stain across cardiac compartments, quantified using ImageJ software***

Compartment	Control	Obese	Tirzepatide	Semaglutide
Cardiac valve [%]	4.2±0.8^{a}	18.6±2.4^{b}	5.1±1.0^{a}	9.8±1.6^{c}
Ventricular myocardium [%]	3.1±0.6^{a}	14.3±2.1^{b}	3.8±0.9^{a}	7.9±1.3^{c}
Coronary artery [%]	5.6±1.1^{a}	21.4±3.0^{b}	6.3±1.2^{a}	11.2±2.0^{c}

Group order: control, obese, tirzepatide, semaglutide (n=10/group). Values are mean ± SD. ^{a,b,c}Within a row, groups sharing the same superscript letter do not differ significantly (Tukey's HSD *post-hoc* test, α=0.05). HSD: Honestly significant difference; MT: Masson's trichrome; n: No. of animals; SD: Standard deviation.

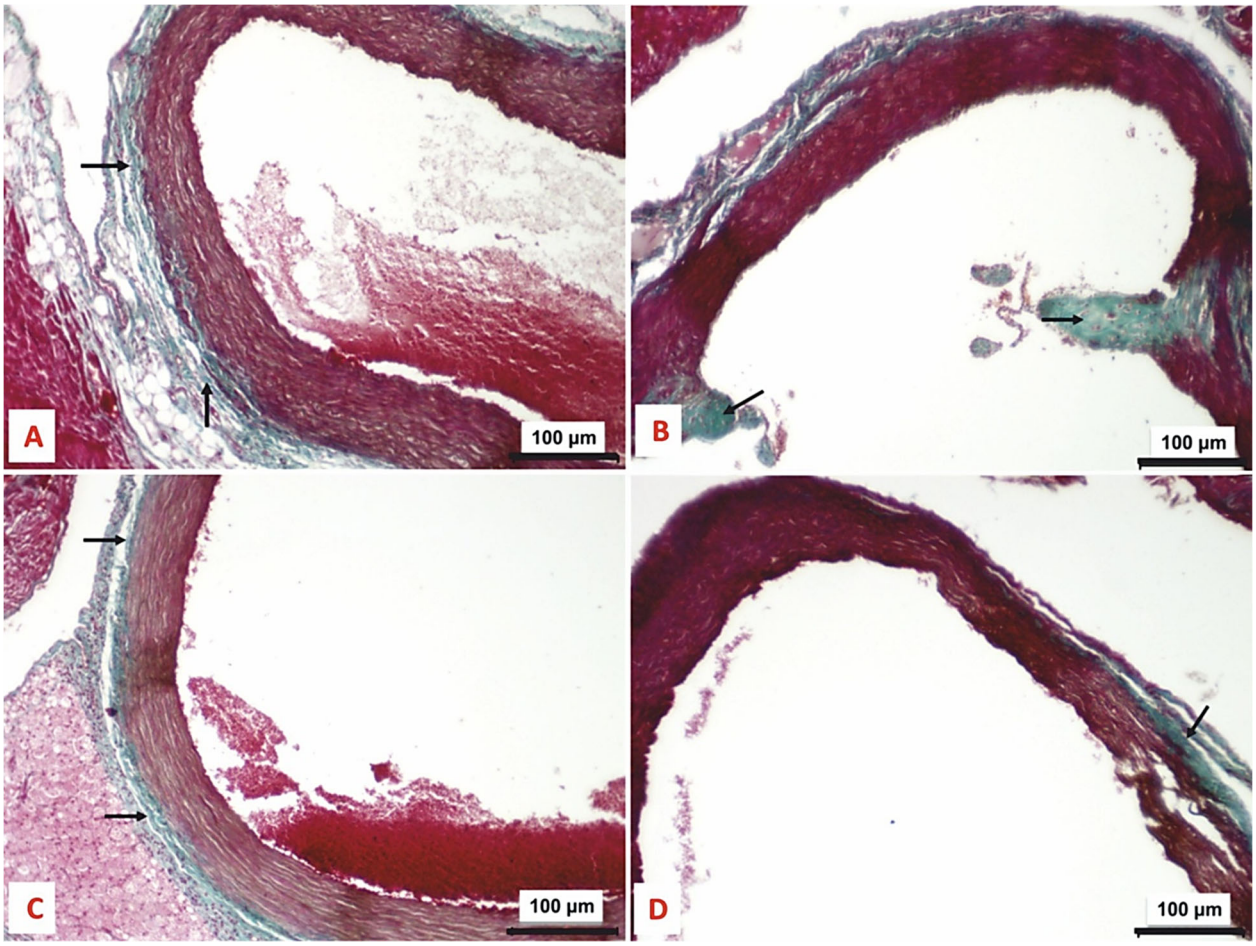

Figure 7 – ***MT staining of coronary artery: (A) Control group showing normal distribution of collagen fibers confined to the tunica adventitia (black arrows), with no collagen in the tunica intima or media; (B) Obese group showing abnormal deposition of thick collagen fibers in the tunica intima (black arrows); (C) Semaglutide group showing largely restored distribution of collagen fibers in the tunica adventitia (black arrow) with minimal residual intimal collagen; (D) Tirzepatide group showing collagen distribution largely confined to the tunica adventitia (black arrow), similar to the control group. Scale bar: (A–D) 100 µm. MT: Masson's trichrome.***

Immunohistochemical markers

CD31 (endothelial marker)

Control group

Cardiac sections demonstrated low CD31 immunoreactivity (brown staining) on endothelial cells lining blood vessels, consistent with physiological vascular density in normal cardiac tissue (Figure 8A).

Obese group

CD31 immunoreactivity remained low, without evidence of the increase in vascular density that would be expected if compensatory angiogenesis had occurred, despite the presence of perivascular fibrosis (Figure 8B).

Semaglutide-treated group

Few CD31-positive structures were detected, a modest increase relative to the obese group (Figure 8C).

Tirzepatide-treated group

Stronger and more widespread CD31 immunoreactivity was observed throughout the myocardium than in the other three groups (Figure 8D).

CD36 (fatty acid translocase)

Control group

Low CD36 immunoreactivity was detected at the cardiomyocyte cell membrane, representing baseline physiological FA uptake (Figure 9A).

Obese group

High CD36 immunoreactivity was observed as strong brown staining at the cell membranes of cardiomyocytes, a pattern reported to accompany increased FA uptake in other models of lipid overload; direct measurement of myocardial lipid content [e.g., triglyceride (TG) assay or Oil Red O staining] was not performed here to confirm lipotoxic substrate accumulation (Figure 9B).

Semaglutide-treated group

Moderate CD36 immunoreactivity remained in cardiomyocyte membranes, intermediate between the obese and control groups (Figure 9C).

Tirzepatide-treated group

CD36 immunoreactivity was reduced to levels comparable to controls (Figure 9D).

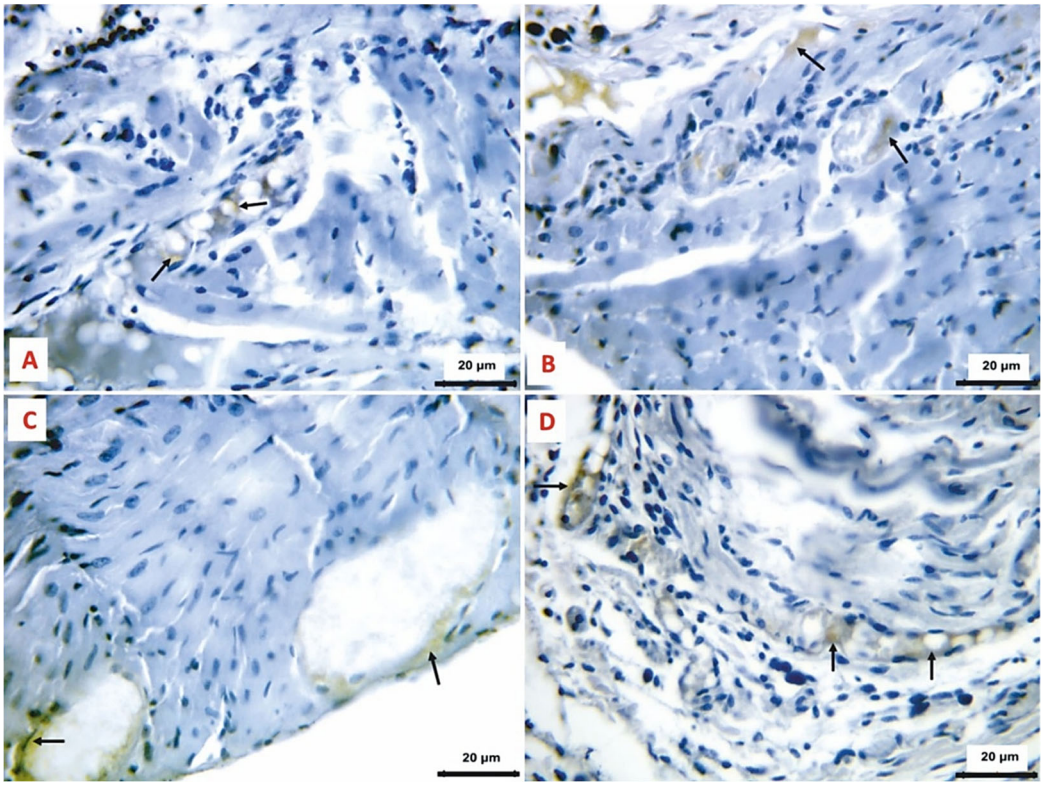

Figure 8 – ***IHC staining for CD31 in cardiac tissue: (A) Control group showing low baseline immunoreactivity (brown staining, black arrows) localizing to endothelial cells of normal blood vessels; (B) Obese group showing persistently low CD31 immunoreactivity (brown staining, black arrows) in blood vessels; (C) Semaglutide group showing a few CD31-positive structures (brown staining, black arrows); (D) Tirzepatide-treated group showing more numerous, strongly CD31-positive structures (brown staining, black arrows). Scale bar: (A–D) 20 µm. CD31: Cluster of differentiation 31; IHC: Immunohistochemical.***

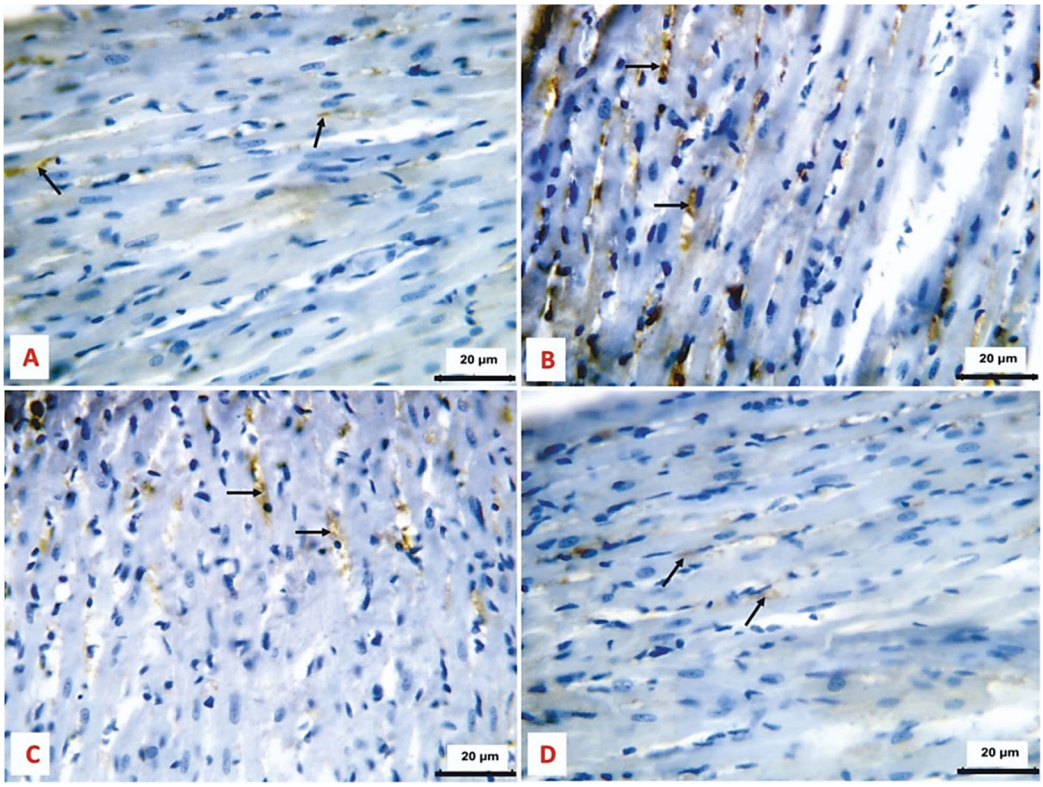

Figure 9 – ***IHC staining for CD36 in cardiac tissue: (A) Control group showing low immunoreactivity (brown staining, black arrows) at the cell membrane of cardiomyocytes; (B) Obese group showing high immunoreactivity (strong brown staining, black arrows); (C) Semaglutide group showing moderate immunoreactivity (brown staining, black arrows); (D) Tirzepatide-treated rats showing low immunoreactivity (brown staining, black arrows). Scale bar: (A–D) 20 µm. CD36: Cluster of differentiation 36; IHC: Immunohistochemical.***

CD86 (macrophage co-stimulatory marker)

Control group

CD86 immunostaining was negative, consistent with the absence of a substantial population of CD86-expressing cells in normal cardiac tissue (Figure 10A).

Obese group

Strong, positive CD86 immunoreactivity was detected in cells distributed within the cardiac interstitium, morphologically consistent with infiltrating macrophages (Figure 10B).

Semaglutide-treated group

Focal, positive CD86 immunoreactivity was observed in scattered cells within the interstitium, intermediate between the obese and control/tirzepatide groups (Figure 10C).

Tirzepatide-treated group

CD86 immunoreactivity was reduced below the detection threshold of this assay (Figure 10D).

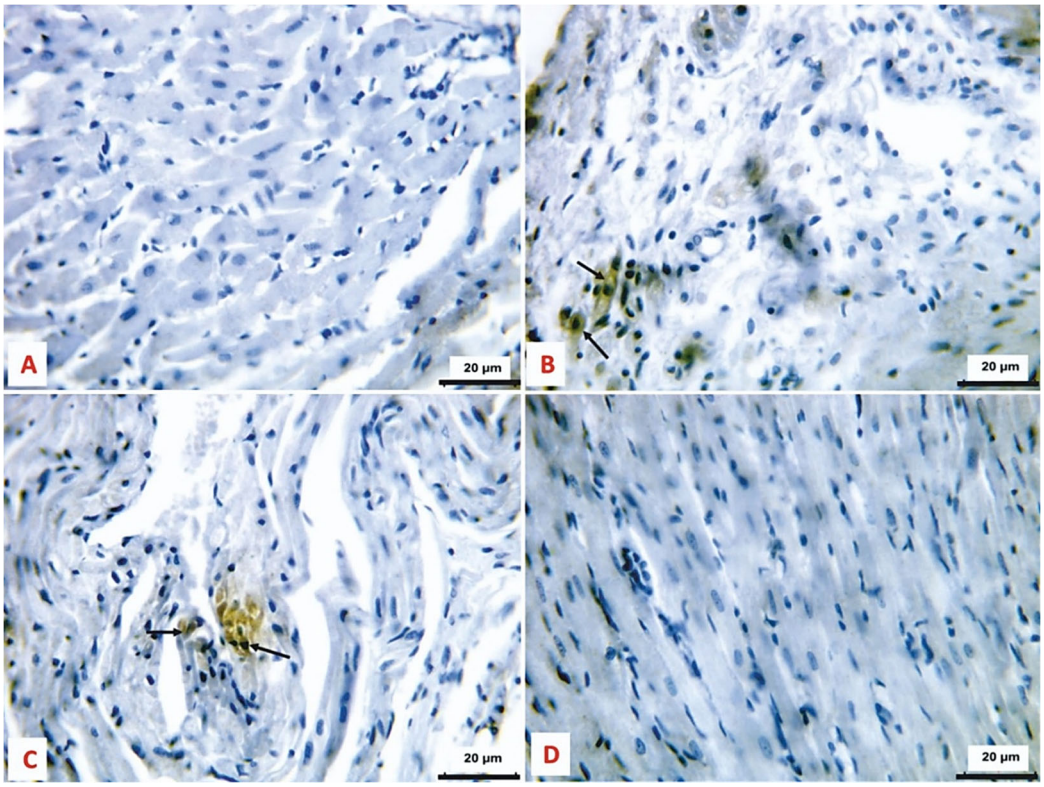

Figure 10 – ***IHC staining for CD86 in cardiac tissue: (A) Control group showing negative expression; (B) Obese group showing strong, positive immunoreactivity (brown staining, black arrows) in cells within the cardiac interstitium; (C) Semaglutide group showing focal, positive immunoreactivity (brown staining, black arrows) in scattered cells; (D) Tirzepatide group showing immunoreactivity reduced below the detection threshold of this assay. Scale bar: (A–D) 20 µm. CD86: Cluster of differentiation 86; IHC: Immunohistochemical.***

ImageJ quantification of immunohistochemical markers

The DAB-positive area for CD31, CD36, and CD86 was quantifiable by digital ImageJ across all groups, and was concordant with the semi-quantitative visual assessment, with the DAB-positive area highest for CD31 in the hearts treated with tirzepatide and lowest in the obese group, and the area highest for CD36 and lowest for CD86 in the hearts of the obese group (Table 3).

Table 3 – ***ImageJ-quantified IHC analysis: percentage DAB-positive area and IOD for CD31, CD36, and CD86***

Immunomarker	Parameter	Control	Obese	Tirzepatide	Semaglutide	*F* (3, 36)	*p*	η^2
CD31	% DAB area	3.2±0.7^{a}	3.5±0.8^{a}	18.9±2.6^{c}	8.4±1.5^{b}	212.0	<0.001	0.946
CD31	IOD (a.u.)	0.045±0.010^{a}	0.048±0.011^{a}	0.187±0.021^{c}	0.096±0.014^{b}	204.7	<0.001	0.945
CD36	% DAB area	4.1±0.9^{a}	22.7±3.2^{c}	5.0±1.1^{a}	13.6±2.0^{b}	186.0	<0.001	0.939
CD36	IOD (a.u.)	0.052±0.012^{a}	0.234±0.028^{c}	0.061±0.013^{a}	0.142±0.019^{b}	197.2	<0.001	0.943
CD86	% DAB area	0.8±0.3^{a}	19.5±2.9^{c}	0.9±0.4^{a}	7.2±1.4^{b}	291.1	<0.001	0.960
CD86	IOD (a.u.)	0.010±0.004^{a}	0.201±0.025^{c}	0.011±0.005^{a}	0.081±0.012^{b}	398.9	<0.001	0.971

Group order: control, obese, tirzepatide, semaglutide (n=10/group). Values are mean ± SD. ^{a,b,c}Within a row, groups sharing a superscript letter do not differ significantly (Tukey's HSD *post-hoc* test, α=0.05). Letters run from lowest (^{a}) to highest (^{c}). CD: Cluster of differentiation; DAB: 3,3,'-Diaminobenzidine; HSD: Honestly significant difference; IHC: Immunohistochemical; IOD: Integrated optical density; *n*: No. of animals; SD: Standard deviation.

Discussions

This study compares and describes in detail the cardiac tissue alterations in what is essentially an obese Wistar rat model that consumed an HFD and was treated with either daily s.c. tirzepatide or semaglutide in a histological and IHC manner. We found both agents to be associated with improvement in the measured obesity-associated cardiac changes, and tirzepatide had numerically larger changes in all parameters assessed.

The successful induction of obesity by HFD was confirmed by significantly higher body weight in all HFD groups at treatment baseline (≥20% above controls), consistent with established rodent obesity models [22, 38]. The progressive weight reduction in both drug groups, reaching values close to control by week 4, is consistent with the known appetite-suppressing and gastric-emptying effects of GLP-1 receptor activation [39, 40]. The similar body weight outcome between the tirzepatide and semaglutide groups in this four-week, daily-dosing model is not directly comparable to the SURMOUNT-5 trial, in which tirzepatide produced significantly greater weight and waist-circumference reduction than semaglutide over 72 weeks of once-weekly dosing at maximum tolerated clinical doses [17]; the discrepancy may reflect the shorter duration, the non-equivalent daily dosing regimen used here, and/or a ceiling effect at near-control body weights in both treated groups in this model, rather than true pharmacological equivalence between the two drugs.

The histological findings in obese rats' clear spaces morphologically consistent with adipocytes within the valve *spongiosa*, inflammatory cell clustering, and layer thickening – resemble patterns described in the obesity-related valvulopathy literature [41, 42]. If confirmed as adipose tissue, such infiltration could plausibly disrupt the proteoglycan matrix responsible for valve leaflet flexibility; this mechanism is proposed as a hypothesis rather than demonstrated directly in this study. The more complete regulation of valve architecture observed with tirzepatide compared with semaglutide could be consistent with an additional anti-inflammatory effect of GIP receptor co-agonism, since GIP has been reported to limit monocyte/macrophage activation in vascular tissue [43], but this mechanistic explanation was not directly tested here and should be regarded as speculative.

MT findings, supported by the ImageJ-derived collagen area fraction measurements, showed that HFD feeding was associated with increased collagen in all three cardiac compartments examined: the valve, the perivascular and interstitial myocardium, and the coronary artery intima – a pattern that, in other contexts, has been associated with early atherosclerotic remodeling, although this was not independently confirmed here [44, 45]. Myocardial interstitial fibrosis in obesity has been linked to transforming growth factor-beta 1 (TGF-β_1) activation of cardiac fibroblasts, amplified by macrophage-derived profibrotic cytokines in other models [46]. The larger reduction in myocardial and coronary collagen area fraction with tirzepatide compared with semaglutide is consistent with more effective suppression of this fibrotic process, and GIP receptor-mediated modulation of macrophage-driven inflammatory and matrix-remodeling signaling is one plausible mechanism reported elsewhere [43]; however, TGF-β signaling was not measured in this study, and this remains a hypothesis for future mechanistic work rather than a demonstrated pathway.

The higher serum and tissue MCP-1 in obese rats is consistent with cardiac monocyte recruitment and inflammatory activation described in obesity-associated cardiac remodeling [8, 11]. MCP-1 is produced by cardiomyocytes, endothelial cells, and adipose tissue and contributes to macrophage recruitment into the myocardium in other models [8, 36]. The modest decrease in MCP-1 with tirzepatide may reflect its reduced immunoreactivity of CD86 and is consistent with greater effects on the upstream inflammatory pathway (*via* GIP receptor activity on myeloid cells) than with selective GLP-1 receptor stimulation; the molecular mechanism underlying this difference was not investigated in this study.

In the obese group, increased CD36 immunoreactivity in cardiomyocytes is consistent with a shift toward increased myocardial FA uptake, a process that, when it exceeds mitochondrial oxidative capacity in other models, has been linked to oxidative stress and cardiomyocyte apoptosis [6, 7, 47]; this specific sequence of events was not measured directly here. GLP-1 receptor stimulation has been reported to reduce CD36 expression through cyclic adenosine monophosphate (cAMP)-related signaling in macrophages, and GIP receptor co-agonism has been proposed to provide an additional inhibitory input [48]; the more complete reduction in CD36 immunoreactivity observed with tirzepatide in this study is compatible with, but does not on its own confirm, this proposed dual mechanism. CD36 is expressed on multiple cell types besides cardiomyocytes, and membranous *vs.* cytoplasmic localization of staining was not formally distinguished in this analysis; myocardial TG or ceramide measurements would be needed to directly support a lipotoxicity interpretation.

The reduction of CD86 immunoreactivity below the detection threshold with tirzepatide, compared with only a partial reduction with semaglutide, is a notable finding of this study. Because CD86 is not specific to macrophages, this finding is presented descriptively rather than as confirmed evidence of macrophage depletion or of a specific macrophage polarization shift. If confirmed by macrophage lineage co-staining, such a reduction would be consistent with less M1-like macrophage activity, which in other models has been linked to reduced secretion of TNF-α, IL-1β, and matrix metalloproteinases that promote ECM degradation and cardiomyocyte injury [11, 49]. GIP receptor activation on myeloid cells has been proposed in other systems to favor an anti-inflammatory macrophage phenotype through cAMP/protein kinase A (PKA)-related suppression of nuclear factor kappa-light-chain-enhancer of activated B-cells (NF-κB) signaling [43, 50]; this is offered here as a plausible hypothesis for the observed difference between tirzepatide and semaglutide, not as a mechanism demonstrated by the present data, particularly since tissue and serum MCP-1, an upstream chemokine, remained above control levels in the tirzepatide group despite the near-absent CD86 immunostaining, indicating that inflammatory activity was reduced but not necessarily eliminated.

The stronger CD31 immunoreactivity in tirzepatide-treated hearts is a notable observation in this study. CD31/PECAM-1 is expressed on endothelial cells and is

one marker used, among others, to study vascular density and endothelial integrity; by itself, an increase in CD31-positive area does not establish new vessel formation, angiogenesis, endothelial progenitor cell recruitment, or restored perfusion, and could also reflect vascular dilation or differences in field/section sampling [13]. GLP-1 receptor agonism has been reported to support endothelial cell survival and nitric oxide bioavailability in other models [51], and it has been proposed that additional GIP receptor activation may further limit vascular inflammation [43, 48]; however, this study did not include markers of endothelial proliferation (*e.g.*, CD31/Ki-67 double labeling), markers of active angiogenesis [*e.g.*, vascular endothelial growth factor (VEGF)/vascular endothelial growth factor receptor 2 (VEGFR2), CD105], or functional/perfusion measurements, so this proposed mechanism remains a hypothesis to be tested directly in future work rather than a confirmed finding of this study.

Limitations

There are a few key limitations that need to be taken into consideration when interpreting the results of this study.

There were no pair-fed obese groups, weight-matched control groups or vehicle-injected control groups. This design cannot rule out that reduced feeding, weight loss, better insulin sensitivity, lower levels of circulating lipids, a lower level of cardiac workload, or unequal handling/injection stress of the animals between the obese and the treated groups is responsible for the observed histological or biomarker differences.

Both drugs were given once daily, instead of once a week as recommended in the label. This was attributed to their significantly shorter plasma half-life in rats as compared to humans [24, 25]. The two doses were chosen from the cited preclinical literature, however, and it is possible that any differences seen are the result of different relative doses of the two agents and not due to a true pharmacodynamic difference.

Body weight and heart weight were the main characteristics used to describe obesity and how to overcome it. No measurements were made of fasting glucose, insulin or insulin-resistance indices, TGs and cholesterol, circulating free FAs, adiposity/fat-pad mass, blood pressure, cardiac functional assessment (echocardiography), ventricular wall thickness, and cardiomyocyte cross-sectional area. This metabolic and functional characterization is not adequate for a diagnosis of obesity-induced cardiomyopathy, so these findings are referred to as "obesity-associated cardiac histological alterations".

Spaces morphologically interpreted as adipocytes within the valve *spongiosa* were identified by morphology alone on H&E without confirmation using an adipocyte or lipid specific staining (*e.g.*, perilipin immunostaining or Oil Red O on frozen tissue) and processing artifact/incorporation of adjacent epicardial fat cannot be excluded.

Conclusions

In this study, we report multi-compartment histochemical and IHC changes in the cardiac valve, heart ventricular myocardium and coronary arteries of the HFD induced obese rats including structural disruption of cardiac valve architecture, increased collagen area fraction in all three compartments, increased CD36 and CD86 immunoreactivity, elevated serum and tissue MCP-1, reduced CD31 immunoreactivity and increased absolute weight of the heart. Tirzepatide and semaglutide both improved these changes, and there was a numerically greater improvement with tirzepatide for all histological, IHC and biochemical parameters assessed.

Conflict of interests

The authors declare no conflict of interests relevant to this study.

Acknowledgements

The authors gratefully acknowledge the technical assistance of the staff of the Animal Care Facility in the College of Veterinary Medicine and the Postgraduate Research Laboratory in the College of Medicine, University of Mosul, Iraq. No external or commercial funding was received for this study. All drugs were purchased commercially using institutional research funds.

References

[1] World Health Organization (WHO). Obesity and overweight. WHO, Geneva, Switzerland, 7 October 2026. https://www.who.int/news-room/fact-sheets/detail/obesity-and-overweight

[2] Boutari C, Mantzoros CS. A 2022 update on the epidemiology of obesity and a call to action: as its twin COVID-19 pandemic appears to be receding, the obesity and dysmetabolism pandemic continues to rage on. Metabolism, 2022, 133:155217. https://doi.org/10.1016/j.metabol.2022.155217 PMID: 35584732 PMCID: PMC9107388

[3] Koliaki C, Liatis S, Kokkinos A. Obesity and cardiovascular disease: revisiting an old relationship. Metabolism, 2019, 92: 98–107. https://doi.org/10.1016/j.metabol.2018.10.011 PMID: 30399375

[4] Nakamura M, Sadoshima J. Mechanisms of physiological and pathological cardiac hypertrophy. Nat Rev Cardiol, 2018, 15(7): 387–407. https://doi.org/10.1038/s41569-018-0007-y PMID: 29674714

[5] Packer M. Epicardial adipose tissue may mediate deleterious effects of obesity and inflammation on the myocardium. J Am Coll Cardiol, 2018, 71(20):2360–2372. https://doi.org/10.1016/j.jacc.2018.03.509 PMID: 29773163

[6] Glatz JFC, Luiken JJFP. Dynamic role of the transmembrane glycoprotein CD36 (SR-B2) in cellular fatty acid uptake and utilization. J Lipid Res, 2018, 59(7):1084–1093. https://doi.org/10.1194/jlr.r082933 PMID: 29627764 PMCID: PMC6027920

[7] Goldberg IJ, Trent CM, Schulze PC. Lipid metabolism and toxicity in the heart. Cell Metab, 2012, 15(6):805–812. https://doi.org/10.1016/j.cmet.2012.04.006 PMID: 22682221 PMCID: PMC3387529

[8] Kanda H, Tateya S, Tamori Y, Kotani K, Hiasa K, Kitazawa R, Kitazawa S, Miyachi H, Maeda S, Egashira K, Kasuga M. MCP-1 contributes to macrophage infiltration into adipose tissue, insulin resistance, and hepatic steatosis in obesity. J Clin Invest, 2006, 116(6):1494–1505. https://doi.org/10.1172/JCI26498 PMID: 16691291 PMCID: PMC1459069

[9] Gu L, Okada Y, Clinton SK, Gerard C, Sukhova GK, Libby P, Rollins BJ. Absence of monocyte chemoattractant protein-1 reduces atherosclerosis in low density lipoprotein receptor-deficient mice. Mol Cell, 1998, 2(2):275–281. https://doi.org/10.1016/s1097-2765(00)80139-2 PMID: 9734366

[10] Lavine KJ, Epelman S, Uchida K, Weber KJ, Nichols CG, Schilling JD, Ornitz DM, Randolph GJ, Mann DL. Distinct macrophage lineages contribute to disparate patterns of cardiac recovery and remodeling in the neonatal and adult heart. Proc Natl Acad Sci U S A, 2014, 111(45):16029–16034. https://doi.org/10.1073/pnas.1406508111 PMID: 25349429 PMCID: PMC4234568

[11] Hulsmans M, Sam F, Nahrendorf M. Monocyte and macrophage contributions to cardiac remodeling. J Mol Cell Cardiol, 2016, 93:149–155. https://doi.org/10.1016/j.yjmcc.2015.11.015 PMID: 26593722 PMCID: PMC4846552

[12] Paulus WJ, Tschöpe C. A novel paradigm for heart failure with preserved ejection fraction: comorbidities drive myocardial dysfunction and remodeling through coronary microvascular endothelial inflammation. J Am Coll Cardiol, 2013, 62(4):263–271. https://doi.org/10.1016/j.jacc.2013.02.092 PMID: 23684677
[13] Newman PJ. The biology of PECAM-1. J Clin Invest, 1997, 100(11 Suppl):S25–S29. PMID: 9413397
[14] Marso SP, Bain SC, Consoli A, Eliaschewitz FG, Jódar E, Leiter LA, Lingvay I, Rosenstock J, Seufert J, Warren ML, Woo V, Hansen O, Holst AG, Pettersson J, Vilsbøll T; SUSTAIN-6 Investigators. Semaglutide and cardiovascular outcomes in patients with type 2 diabetes. N Engl J Med, 2016, 375(19):1834–1844. https://doi.org/10.1056/NEJMoa1607141 PMID: 27633186
[15] Lincoff AM, Brown-Frandsen K, Colhoun HM, Deanfield J, Emerson SS, Esbjerg S, Hardt-Lindberg S, Hovingh GK, Kahn SE, Kushner RF, Lingvay I, Oral TK, Michelsen MM, Plutzky J, Tornøe CW, Ryan DH; SELECT Trial Investigators. Semaglutide and cardiovascular outcomes in obesity without diabetes. N Engl J Med, 2023, 389(24):2221–2232. https://doi.org/10.1056/NEJMoa2307563 PMID: 37952131
[16] Jastreboff AM, Aronne LJ, Ahmad NN, Wharton S, Connery L, Alves B, Kiyosue A, Zhang S, Liu B, Bunck MC, Stefanski A; SURMOUNT-1 Investigators. Tirzepatide once weekly for the treatment of obesity. N Engl J Med, 2022, 387(3):205–216. https://doi.org/10.1056/NEJMoa2206038 PMID: 35658024
[17] Aronne LJ, Horn DB, le Roux CW, Ho W, Falcon BL, Gomez Valderas E, Das S, Lee CJ, Glass LC, Senyucel C, Dunn JP; SURMOUNT-5 Trial Investigators. Tirzepatide as compared with semaglutide for the treatment of obesity. N Engl J Med, 2025, 393(1):26–36. https://doi.org/10.1056/NEJMoa2416394 PMID: 40353578
[18] Frías JP, Davies MJ, Rosenstock J, Pérez Manghi FC, Fernández Landó L, Bergman BK, Liu B, Cui X, Brown K; SURPASS-2 Investigators. Tirzepatide *versus* semaglutide once weekly in patients with type 2 diabetes. N Engl J Med, 2021, 385(6):503–515. https://doi.org/10.1056/NEJMoa2107519 PMID: 34170647
[19] Baggio LL, Drucker DJ. Biology of incretins: GLP-1 and GIP. Gastroenterology, 2007, 132(6):2131–2157. https://doi.org/10.1053/j.gastro.2007.03.054 PMID: 17498508
[20] Drucker DJ. The biology of incretin hormones. Cell Metab, 2006, 3(3):153–165. https://doi.org/10.1016/j.cmet.2006.01.004 PMID: 16517403
[21] National Research Council. Guide for the care and use of laboratory animals. 8th edition, National Academies Press, Washington, DC, USA, 2011. https://www.ncbi.nlm.nih.gov/books/NBK54040/
[22] Sequeira V, Theisen J, Ermer KJ, Oertel M, Xu A, Weissman D, Ecker K, Dudek J, Fassnacht M, Nickel A, Kohlhaas M, Maack C, Dischinger U. Semaglutide normalizes increased cardiomyocyte calcium transients in a rat model of high fat diet-induced obesity. ESC Heart Fail, 2025, 12(2):1386–1397. https://doi.org/10.1002/ehf2.15152 PMID: 39482267 PMCID: PMC11911617
[23] Alathary AJ, Kadhim ZJ. Tirzepatide protects against hepatic oxidative stress in high-fat induced obesity in male rats. Maaen J Med Sci, 2024, 3(3):6. https://doi.org/10.55810/2789-9136.1053
[24] Lee TS, Park EJ, Choi M, Oh HS, An Y, Kim T, Kim TH, Shin BS, Shin S. Novel LC–MS/MS analysis of the GLP-1 analog semaglutide with its application to pharmacokinetics and brain distribution studies in rats. J Chromatogr B Analyt Technol Biomed Life Sci, 2023, 1221:123688. https://doi.org/10.1016/j.jchromb.2023.123688 PMID: 36989942
[25] Song S, Hyeon M, Kim S, Kang Y, Hahm S, Park EB, Shin BS, Shin S. A sensitive LC–MS/MS method for tirzepatide in rat plasma with comprehensive pharmacokinetic evaluation. J Anal Sci Technol, 2026, 17(1):19. https://doi.org/10.1186/s40543-026-00540-5
[26] Panchal SK, Brown L. Rodent models for metabolic syndrome research. J Biomed Biotechnol, 2011, 2011:351982. https://doi.org/10.1155/2011/351982 PMID: 21253582 PMCID: PMC3018657
[27] Buettner R, Schölmerich J, Bollheimer LC. High-fat diets: modeling the metabolic disorders of human obesity in rodents. Obesity (Silver Spring), 2007, 15(4):798–808. https://doi.org/10.1038/oby.2007.608 PMID: 17426312
[28] American Veterinary Medical Association (AVMA). AVMA guidelines for the euthanasia of animals: 2020 edition. AVMA, Schaumburg, IL, USA, 2020. https://www.avma.org/sites/default/files/2020-02/Guidelines-on-Euthanasia-2020.pdf
[29] González A, Schelbert EB, Díez J, Butler J. Myocardial interstitial fibrosis in heart failure: biological and translational perspectives. J Am Coll Cardiol, 2018, 71(15):1696–1706. https://doi.org/10.1016/j.jacc.2018.02.021 PMID: 29650126
[30] Ramos-Vara JA, Miller MA. When tissue antigens and antibodies get along: revisiting the technical aspects of immunohistochemistry – the red, brown, and blue technique. Vet Pathol, 2014, 51(1):42–87. https://doi.org/10.1177/0300985813505879 PMID: 24129895
[31] Schneider CA, Rasband WS, Eliceiri KW. NIH Image to ImageJ: 25 years of image analysis. Nat Methods, 2012, 9(7):671–675. https://doi.org/10.1038/nmeth.2089 PMID: 22930834 PMCID: PMC5554542
[32] Chen Y, Yu Q, Xu CB. A convenient method for quantifying collagen fibers in atherosclerotic lesions by ImageJ software. Int J Clin Exp Med, 2017, 10(10):14904–14910. https://e-century.us/files/ijcem/10/10/ijcem0059973.pdf
[33] Varghese F, Bukhari AB, Malhotra R, De A. IHC Profiler: an open source plugin for the quantitative evaluation and automated scoring of immunohistochemistry images of human tissue samples. PLoS One, 2014, 9(5):e96801. https://doi.org/10.1371/journal.pone.0096801 PMID: 24802416 PMCID: PMC4011881
[34] Ruifrok AC, Johnston DA. Quantification of histochemical staining by color deconvolution. Anal Quant Cytol Histol, 2001, 23(4):291–299. PMID: 11531144
[35] Harikrishnan VS, Hansen AK, Abelson KS, Sørensen DB. A comparison of various methods of blood sampling in mice and rats: effects on animal welfare. Lab Anim, 2018, 52(3):253–264. https://doi.org/10.1177/0023677217741332 PMID: 29165033
[36] Melgarejo E, Medina MÁ, Sánchez-Jiménez F, Urdiales JL. Monocyte chemoattractant protein-1: a key mediator in inflammatory processes. Int J Biochem Cell Biol, 2009, 41(5):998–1001. https://doi.org/10.1016/j.biocel.2008.07.018 PMID: 18761421
[37] Field A. Discovering statistics using IBM SPSS statistics. 5th edition, SAGE Publications, London, UK, 2018. https://search.worldcat.org/title/Discovering-statistics-using-IBM-SPSS-statistics/oclc/1015821231
[38] Hariri N, Thibault L. High-fat diet-induced obesity in animal models. Nutr Res Rev, 2010, 23(2):270–299. https://doi.org/10.1017/s0954422410000168 PMID: 20977819
[39] Wilding JPH, Batterham RL, Calanna S, Davies M, Van Gaal LF, Lingvay I, McGowan BM, Rosenstock J, Tran MTD, Wadden TA, Wharton S, Yokote K, Zeuthen N, Kushner RF; STEP 1 Study Group. Once-weekly semaglutide in adults with overweight or obesity. N Engl J Med, 2021, 384(11):989–1002. https://doi.org/10.1056/NEJMoa2032183 PMID: 33567185
[40] Nauck MA, Quast DR, Wefers J, Meier JJ. GLP-1 receptor agonists in the treatment of type 2 diabetes – state-of-the-art. Mol Metab, 2021, 46:101102. https://doi.org/10.1016/j.molmet.2020.101102 PMID: 33068776 PMCID: PMC8085572
[41] Larsson SC, Wolk A, Håkansson N, Bäck M. Overall and abdominal obesity and incident aortic valve stenosis: two prospective cohort studies. Eur Heart J, 2017, 38(28):2192–2197. https://doi.org/10.1093/eurheartj/ehx140 PMID: 28402538 PMCID: PMC5837465
[42] Kaltoft M, Langsted A, Nordestgaard BG. Obesity as a causal risk factor for aortic valve stenosis. J Am Coll Cardiol, 2020, 75(2):163–176. https://doi.org/10.1016/j.jacc.2019.10.050 PMID: 31948645
[43] Kahles F, Liberman A, Halim C, Rau M, Möllmann J, Mertens RW, Rückbeil M, Diepolder I, Walla B, Diebold S, Burgmaier M, Lebherz C, Marx N, Lehrke M. The incretin hormone GIP is upregulated in patients with atherosclerosis and stabilizes plaques in ApoE$^{-/-}$ mice by blocking monocyte/macrophage activation. Mol Metab, 2018, 14:150–157. https://doi.org/10.1016/j.molmet.2018.05.014 PMID: 29884547 PMCID: PMC6034034
[44] Bäck M, Yurdagul A Jr, Tabas I, Öörni K, Kovanen PT. Inflammation and its resolution in atherosclerosis: mediators and therapeutic opportunities. Nat Rev Cardiol, 2019, 16(7):389–406. https://doi.org/10.1038/s41569-019-0169-2 PMID: 30846875 PMCID: PMC6727648

[45] Frangogiannis NG. Cardiac fibrosis. Cardiovasc Res, 2021, 117(6):1450–1488. https://doi.org/10.1093/cvr/cvaa324 PMID: 33135058 PMCID: PMC8152700
[46] Frangogiannis NG. Transforming growth factor-β in myocardial disease. Nat Rev Cardiol, 2022, 19(7):435–455. https://doi.org/10.1038/s41569-021-00646-w PMID: 34983937
[47] Fillmore N, Mori J, Lopaschuk GD. Mitochondrial fatty acid oxidation alterations in heart failure, ischaemic heart disease and diabetic cardiomyopathy. Br J Pharmacol, 2014, 171(8): 2080–2090. https://doi.org/10.1111/bph.12475 PMID: 24147975 PMCID: PMC3976623
[48] Nagashima M, Watanabe T, Terasaki M, Tomoyasu M, Nohtomi K, Kim-Kaneyama J, Miyazaki A, Hirano T. Native incretins prevent the development of atherosclerotic lesions in apolipoprotein E knockout mice. Diabetologia, 2011, 54(10): 2649–2659. https://doi.org/10.1007/s00125-011-2241-2 PMID: 21786155 PMCID: PMC3168747
[49] Murray PJ, Allen JE, Biswas SK, Fisher EA, Gilroy DW, Goerdt S, Gordon S, Hamilton JA, Ivashkiv LB, Lawrence T, Locati M, Mantovani A, Martinez FO, Mege JL, Mosser DM, Natoli G, Saeij JP, Schultze JL, Shirey KA, Sica A, Suttles J, Udalova I, van Ginderachter JA, Vogel SN, Wynn TA. Macrophage activation and polarization: nomenclature and experimental guidelines. Immunity, 2014, 41(1):14–20. https://doi.org/10.1016/j.immuni.2014.06.008 PMID: 25035950 PMCID: PMC4123412
[50] Mantelmacher FD, Zvibel I, Cohen K, Epshtein A, Pasmanik-Chor M, Vogl T, Kuperman Y, Weiss S, Drucker DJ, Varol C, Fishman S. GIP regulates inflammation and body weight by restraining myeloid-cell-derived S100A8/A9. Nat Metab, 2019, 1(1):58–69. https://doi.org/10.1038/s42255-018-0001-z PMID: 32694806
[51] Nyström T, Gutniak MK, Zhang Q, Zhang F, Holst JJ, Ahrén B, Sjöholm A. Effects of glucagon-like peptide-1 on endothelial function in type 2 diabetes patients with stable coronary artery disease. Am J Physiol Endocrinol Metab, 2004, 287(6):E1209–E1215. https://doi.org/10.1152/ajpendo.00237.2004

Corresponding author
Harith Ali Hasan, Assistant Lecturer, PhD Student, Department of Anatomy, College of Medicine, University of Mosul, Al Majmoaa Street, 41002 Mosul, Iraq; Phone +964 (60) 812 256, e-mail: harith.hasan@uomosul.edu.iq

Received: July 17, 2026

Accepted: November 2, 2026